Experimental Flow Field Investigation of the Bio-inspired Corrugated Wing and Hybrid Wing for MAV Applications

Y. D. Dwivedi, Abhishek Mohapatra, and Mohammad Irfan

Abstract In this work, the flow behavior of a dragonfly-inspired corrugated wing was undertaken using a subsonic wind tunnel to assess the aerodynamic performance and flow characteristics. The test was performed at Reynolds numbers (Re) 46,000 and 67,000, which is the flying regime of micro aerial vehicles. A wing having the same geometrical dimensions as the midsection of the dragonfly forewing known as corrugated wing and another wing having the same geometry as the first wing without corrugations known as hybrid wing were fabricated using 3-D printing machine. The tufts of three different colors were glued at three locations, i.e., 0, 30, and 60% of the semispan of both wings at the trailing edge to visualize the flow separation and reversal phenomenon. The boundary layer rack was used at these three locations to obtain velocity gradient and boundary layer thickness. The result of the tuft flow visualization showed that the flow pattern at all three locations is not the same for the same Re and angles of attack. At high AOA, the corrugated wing shows lesser velocity gradients than the hybrid wing for both tested Reynolds number. The results clearly demonstrate that the bio-inspired corrugated wing surpassed the hybrid wing by delaying the stall up to 28%.

Keywords Bio-inspired wing · Boundary layer · Tuft flow visualization · Stall angle · Flow reversal

1 Introduction

For centuries, nature has inspired humans to fly like a bird or wander like an insect in open sky. However, till today humans have not been able to fly like the avians. The primary reason for this issue is the low Reynolds number (Re), on which the birds and insects normally fly. Extensive studies have been conducted to understand the flow behavior and aerodynamic characteristics around the wings or airfoils at high Re, which corresponds to the high speed and large size of the conventional airplanes.

Y. D. Dwivedi (✉) · A. Mohapatra · M. Irfan
Department of Aeronautical Engineering, Institute of Aeronautical Engineering, Hyderabad 500043, India

G. S. V. L. Narasimham et al. (eds.), *Innovations in Mechanical Engineering*,
Lecture Notes in Mechanical Engineering,
https://doi.org/10.1007/978-981-16-7282-8_3

On the other hand, in recent years, small-sized air vehicles like Micro Air Vehicles (MAVs) and small-sized Unmanned Air Vehicles (UAVs) have been developed to undertake tasks like aerial photography, payload delivery, disaster management, and monitoring hazardous places [1–3]. Transportation by automobiles is the main contributor toward the emission of CO_2 which contributes to the emission of greenhouse gases and has posed serious environmental issues [4, 5]. Nowadays, the UAVs, also known as drones, are extensively employed for the delivery of goods and are able to save 90% of the energy while reducing greenhouse emission enormously [6]. It is also observed that the flow field around the wings or airfoils of small aerial vehicles are significantly different from the conventional airplane wings and airfoils [7] because of the low Re of the tiny flights (Re $<10^5$) [8, 9]. In the high Re range, the inertial force prevails and trailing edge vortices are created, and flow becomes unstable, whereas at low Re, the viscous force is dominant and the flow remains stable as well as smooth. As a result, the performance of the streamlined low Reynolds number wings of MAVs/UAVs/birds/insects, etc. will degrade the performance significantly due to its small size and low velocity [10]. Hence, there is an imperative need to redesign the present conventional airfoils for the application of MAVs/UAVs to obtain better flow characteristics and aerodynamic performance in a low Re regime.

A dragonfly is an insect that fit into the family of *Odonata, anisoptera*, which is significantly fast, agile, and has long endurance. This insect can be classified as low Reynolds number flier as the Re of the dragonfly falls between 10^2 and 10^5 [11]. It can fly in gliding as well as the flapping mode and also in combination of both [12]. In the flapping mode, the dragonfly is able to move forward, climb, and also hover. However, flapping requires significant energy consumption. So, the insect can not fly for a long duration and switches to the gliding mode of the flight as this mode requires virtually little or no energy consumption at all [13]. The dragonfly is unique in its effective gliding flight as it is proficient of flying 40 chord lengths and up to 30 s without any significant change in its altitude [14]. Unlike other avian wings' cross-section, which is mostly smooth and cambered surface, the dragonfly wings' cross-section is found to be corrugated in the chord as well as in spanwise direction. Several computational and experimental studies were performed to assess the aerodynamic behavior of corrugated wing and most of the investigations revealed that the corrugated wing performed at par and sometimes even better than the smooth conventional airfoils, especially at low Re flow regimes, in which the dragonfly mostly operates [15–24].

Numerous research have been undertaken to understand the important source of the unexpected enhancement in the aerodynamic performance of the corrugated airfoils/wings when compared with existing smooth wings. Kesel [12], Rees [13], and Murphy [19] observed that the corrugated wings function as streamlined airfoil as the Leading Edge Vortices (LEVs) are trapped inside the trough of the valleys. This makes the flow to be streamlined, leading to the delay in separation of the flow [15, 21, 22]. As a result, the lift is increased and drag is reduced thereby resulting in increased aerodynamic performance. Dwivedi et al. [22, 23] has worked extensively on the experimental study of the flow field around the corrugated airfoils at low Re and observed that the spanwise flow and boundary layers were significantly different

from the conventional smooth wings. Luo and Sun [17] have investigated the effect of corrugation on the generation of the aerodynamic forces and Vergas and Mittal [18] have performed the numerical study to assess the aerodynamic efficiency and have established that the corrugation gives better efficiency than the smooth profile wing. Tang et al. [20] have worked computationally for the 3D wing and concluded that spanwise flow direction could promote the lift and decrease the drag. They have also confirmed that the wings are unstable and the same results have been obtained by Dwivedi et al. [21]. Despite different explanations about the flow field mechanism for the improved aerodynamic performance by the different investigators, all studies unanimously agree that the corrugation of the wing works well in the low Re regime, which indicates that the bio-inspired corrugated wings can be potentially used for the wings of future MAVs/UAVs applications.

The flow separation and flow reversal have been experimentally observed by Tamai et al. [25]. The computational result of Skote [26, 27] and Chen and Skote [28] have revealed that the spanwise flow does exist in the corrugated wings and the 3D flow field persists. Flow separation occurs when the thickness of the boundary layer exceeds the critical value which results in the adverse pressure gradient (APG). Most of the earlier investigations only focused on comparing the camber as well as the thickness of corrugated wings with that of either the flat plate or NACA airfoils or both [12, 13, 19, 21]. However, those comparisons are unrealistic. First, the flat plate does not even have the camber; second, NACA airfoil geometry is starkly different from that of bio-inspired corrugated wings. So, the previous results obtained, either computationally or experimentally, may not be corresponding with real bio-inspired corrugated wings.

The present work aims to experimentally investigate the flow behavior of a bio-inspired corrugated wing and to compare the results with another wing having the same thickness, camber, chord, the aspect ratio of the hybrid wing in which all corrugations are filled with the material. In this paper, the model is tested in a wind tunnel by varying AOA and two Reynolds numbers 46,000 and 67,000. The flow phenomena of both the tested wings were visualized by using tufts and boundary layers were measured by using boundary layer rake at three different semispan locations in a low speed wind tunnel at 0.7 chord length (70%) from the leading edge of the wing. The flow visualization and boundary layer study will give the clear understanding of the underlying flow mechanism of the bio-inspired corrugated wing and the wing is assessed for the suitability for future use in the MAVs/UAVs application.

2 Methodology

2.1 Materials and Methods

Two different wing models were used in the present study: (1) Corrugated wing and (2) Hybrid wing. Both wing models have the same projected planform area (S), mean

Table 1 Coordinates of corrugated wing profile

Upper surface		Lower surface	
x/c	y/c	x/c	y/c
0	0.02	0.995	−0.02
0.066	0.02	0.912	−0.005
0.124	0.058	0.833	0
0.189	0.016	0.77	−0.028
0.271	0.073	0.688	0.001
0.341	0.013	0.606	−0.027
0.398	0.051	0.537	0.014
0.553	0.051	0.415	0.014
0.61	0.015	0.337	−0.03
0.689	0.043	0.272	0.023
0.772	0.014	0.187	−0.029
0.839	0.032	0.128	0.01
0.897	0.036	0.08	−0.02
1.005	0.02	0	−0.02

chord length (c), and aspect ratio (AR). The construction and design of the profile are based on the real-time analysis of the wing structure of the biological dragonfly under microscopic observation and plotting the spatial locations of the elements of the geometry with respect to the mean chord line of the wing. All the coordinates of the points for corrugated and hybrid profile are given in Tables 1 and 2, respectively, for plotting, design, analysis, and fabrication purposes.

The coordinates (Tables 1 and 2) utilized for plotting the wing geometry (Fig. 1) are gathered from various preexisting sources and are spatially multiplied by the

Table 2 Coordinates of hybrid wing profile

Upper surface		Lower surface	
x/c	y/c	x/c	y/c
0	0.02	0.995	−0.02
0.066	0.02	0.912	−0.005
0.124	0.058	0.833	0
0.271	0.073	0.688	0.001
0.398	0.051	0.537	0.014
0.553	0.051	0.415	0.014
0.689	0.043	0.337	−0.03
0.839	0.032	0.187	−0.029
0.897	0.036	0	−0.02
1.005	0.02		

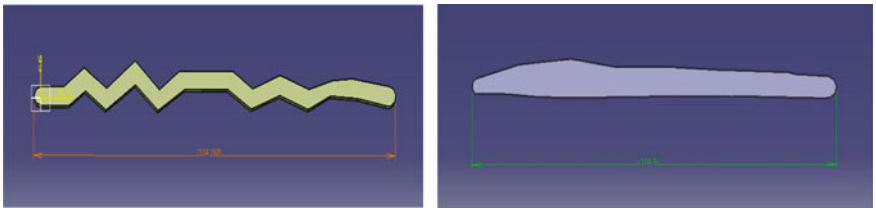

Fig. 1 Geometry of corrugated wing and hybrid wing

suitable integral constants (1:100 scale-up) for a noticeable geometry to carryout aerodynamic analysis using the wind tunnel and obtain important results.

2.1.1 Numerical Adjustments and Curve Fittings

The profile coordinates were refined for plotting suitable corrugated and hybrid wing models for analysis purposes. The real-time wings of dragonflies are too small and to model accurately to its original dimensions would not yield satisfactory results for the wind tunnel testing. The wing tunnel test section (60 cm × 60 cm × 200 cm) is quite huge in magnitude compared to that of a real corrugated wing model of a dragonfly. Such a relatively small wing model would not induce any noticeable disturbances or any significant changes in the free stream flow in the test section. Hence, geometrical enhancements were made to the miniature real dimensions to scale-up (1:100) the reference model to produce significant variations and flow disturbances in the free stream flow within the test section.

The geometrical aberrations are of magnitudes less than 0.15% error to the total dimensions of the model. These profiles were plotted using the aid of the design and modeling software CATIA V5. The generated models (Fig. 2a, b) were then converted into (.stl) format (stereolithography) and G-Code format (RS-274) under standard ISO 6983 conditions. This data of refined coordinates was then used to produce a 3D printed model of Acrylonitrile Butadiene Styrene (ABS) thermoplastic material as shown in Fig. 3.

Model specification includes chord length (c) 0.104 m, wing span 0.205 m, effective thickness 4 mm, and camber 0.17 c. The 3D printing machine (Ultimaker S3) was used to fabricate the model as shown in Fig. 3.

a) Corrugated Wing b) Hybrid Wing

Fig. 2 CATIA 3D model of corrugated (**a**) and hybrid (**b**) wings

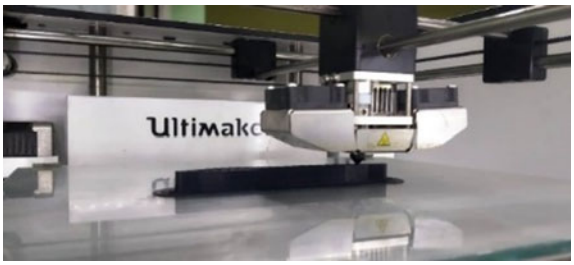

Fig. 3 3D printing of corrugated wings using a Ultimaker S3 3D printer

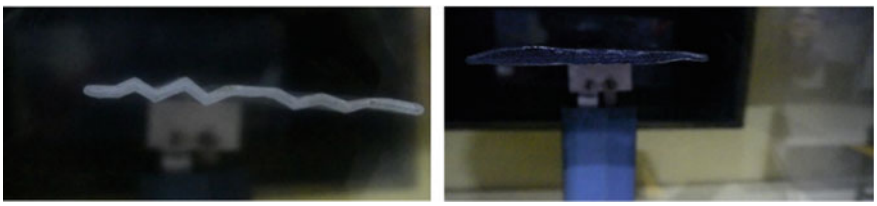

Fig. 4 3D printed wings mounted on six component balance

3 Result and Discussion

3.1 Tuft Flow Visualization

Three different colored tufts were used for both wings tuft flow visualization. Black tuft is fixed at the center of the wing (0%) of semispan (BT 0), red tuft at 30% of semispan (RT 30) and a green tuft at 60% of semispan (GT 60), which is near the tip of the wing.

The experiment was carried out at two-chord Reynolds number (Re_c) 46,000 and 67,000, the angle of attack (AOA) varied from 0° to +20° for both the wings. Chord Reynolds number (Re_c) calculations are given in Table 3. The green tuft (GT 60) located at 60% of semispan toward the tip showed more fluctuations than that of the other two at AoA 20° and Re_c 46,000, while the remaining two, i.e., BT 0 and RT 30 reacted almost similar to the flow (Figs. 5 and 6). In Figs. 7 and 8 at AoA 20° and Re_c 67,000, the flow shows that the flow reversal happened in the hybrid wing in red

Table 3 Chord Reynolds number (Re_c) calculation

Wind tunnel motor RPM	Chord (m)	Wind tunnel velocity (m/s)	Kinematic viscosity (m^2/s)	Chord Reynolds no. (Re_c) (approx.)
265	0.104	6.9089	1.562×10^{-5}	46000
370	0.104	10.0629	1.562×10^{-5}	67000

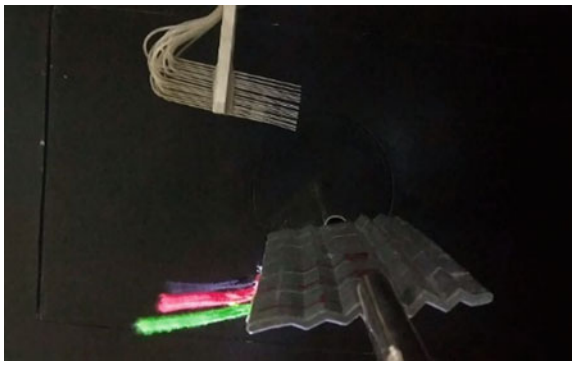

Fig. 5 Tuft flow visualization for corrugated wing at AOA +20° and Re_c 46,000

Fig. 6 Tuft flow visualization for hybrid wing at AOA +20° and Re_c 46,000

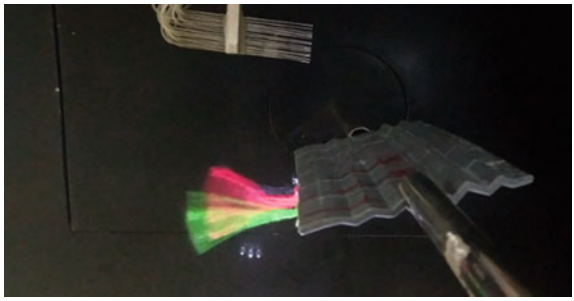

Fig. 7 Tuft flow visualization for corrugated wing at AOA +20° and Rec 67,000

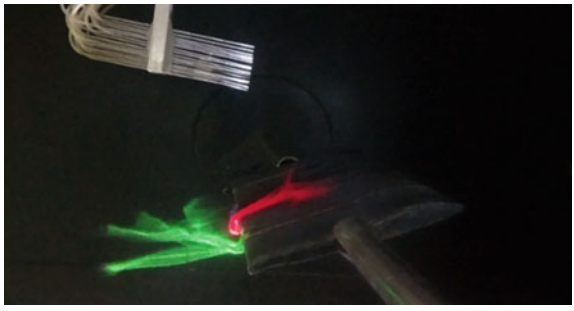

Fig. 8 Tuft flow visualization for hybrid wing at AOA +20° and Rec 67,000

Fig. 9 Flow reversal for corrugated wing at AOA + 18° and Re_c 120,000

Fig. 10 Flow reversal for hybrid wing at AOA +14° and Re_c 120,000

tuft zone first. At this AoA, there is no indication of flow reversal in the corrugated wing.

To observe the clear flow reversal on both the wings, the Re_c was increased further to 120,000, and AoA varied from 0° to +18° and it was found that the hybrid wing flow reversal happened at +14° AoA and flow reversal in corrugated wing happened at +18° of AoA (Figs. 9 and 10). This indicates that the flow separation happened first in the hybrid wing. So, the corrugated wing delays the stall 4° which corresponds to nearly 28% gain in in comparison with hybrid wing.

3.2 Boundary Layer Measurements

In tuft flow visualization, the results were qualitative to find the reversal and separation of the flow for both the wings. However, to find the exact reason which causes flow separation, reversal, and swirling of the flow, a measurement technique was needed. That technique is boundary layer measurement. In boundary layer measurement the target was to obtain the velocity gradients above the two tested wing surfaces at 70% chord length (0.7 c) from the leading edge and at three different semispan

Table 4 Boundary layer rake device probe numbers and distances

Tube no	Distance (mm)	Tube no	Distance (mm)
1	0	10	14.5
2	1.5	11	16.5
3	2.5	12	20.0
4	4.5	13	22.5
5	5.5	14	24.5
6	7.0	15	27.0
7	8.5	16	31.0
8	10.5	17	34.5
9	12.0		

locations at 0, 30, and 60% from the center of the wing. This location has been taken because the tuft flow visualization was done in the same location.

A 17-probe boundary layer measuring rake is used to measure the velocity profile. The location of the each probes is provided in Table 4. The probes were connected to a manometer filled with methanol and aligned perpendicular to the ground, the perpendicular alignment is verified by two-spirit balances attached to the base of the manometer, perpendicular to each other and parallel to the ground. The velocity field around the wing surface creates the pressure difference between the upper and the lower surfaces. However, the variation in the velocity field was not the same for both corrugated and the hybrid wing. Negative pressure was generated on the upper surface of the corrugated wing. The corrugation present at the lower surface acted as a wing camber. The flow behavior observed is completely governed by parameters like chord length, the thickness of profile, AoA, and the relative velocity across the surface of the profile which is responsible for turbulent flow, flow separation, and flow reversal. The boundary layers measurement results from −8°, +4°, and +16° angles of attack and Re_c at 46,000 and 67,000 are given in Figs. 11, 12, 13, 14, 15 and 16.

At AoA −8° and Rec 46,000 and 67,000, the boundary layers and velocity gradient of the corrugated wing are lesser than the hybrid wing (Figs. 11 and 12). The same trends observed at AoA +4 and +16 (Figs. 13, 14, 15 and 16). At +4° AoA and chord Reynolds number at 46,000 the corrugated wing velocity gradient at 30% of the semi wing span was observed to be less than and that of the other two positions. The hybrid wing at the 4° AoA and Rec 46,000 the boundary layer thickness is highest at 60% of semispan, i.e., up to probe number 8, followed by 30% and 0% of the semispan, respectively. It shows that toward the tip of the wing the velocity gradient is higher than the other two locations. However, increasing the Re_c up to 67,000 resulted in the thickest boundary layer at 60% of the wing semispan up to 14th probe, followed by 30% of semispan and 0% of semispan, respectively (Figs. 13 and 14).

At higher AoA, i.e., +16° and Rec 46,000 and 67,000, the trends of boundary layer velocity gradient and thickness are opposite to the −8° and +4° AoA (Figs. 15 and 16). The velocity gradient of the corrugated wing is very less compared to the hybrid

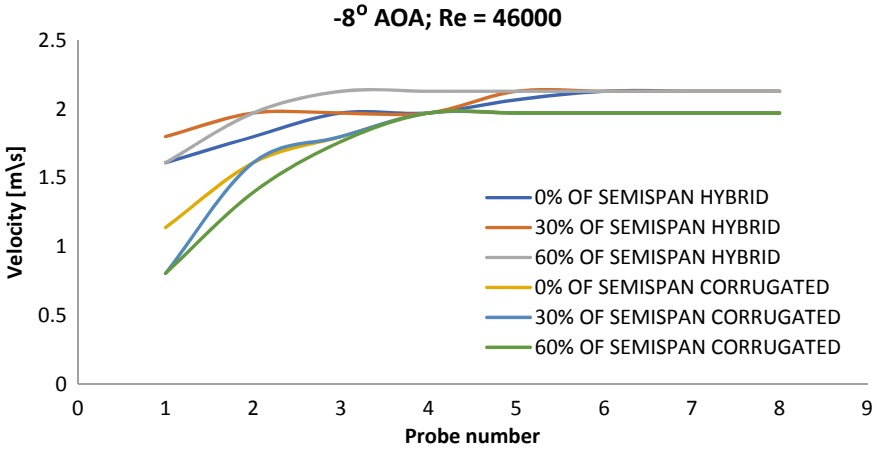

Fig. 11 Comparison of boundary layer velocity at −8° AOA and $Re_c = 46{,}000$

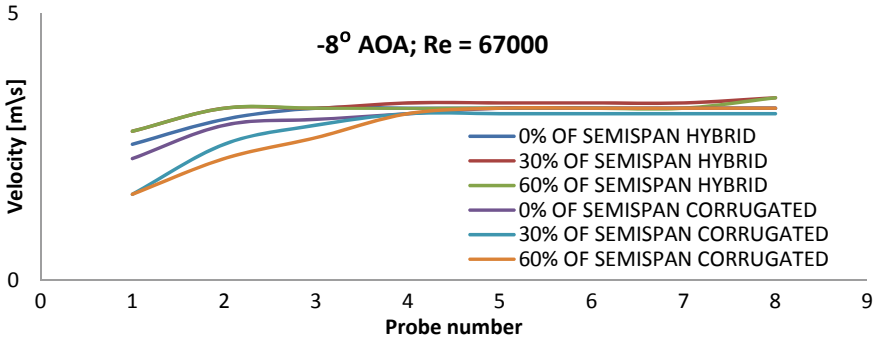

Fig. 12 Comparison of boundary layer velocity at 0° AOA and $Re_c = 67{,}000$

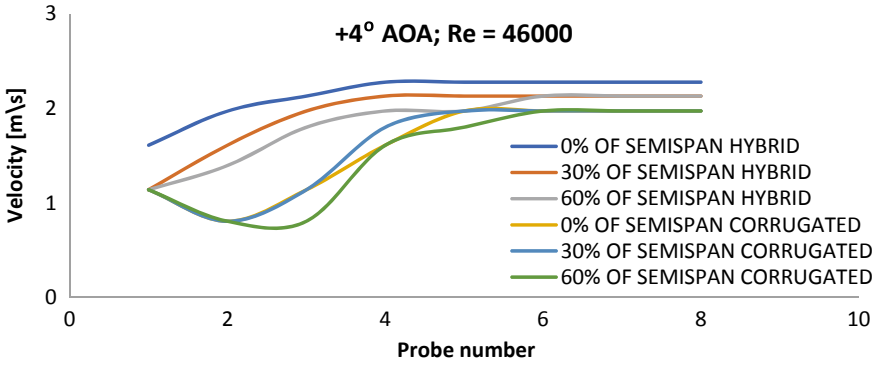

Fig. 13 Comparison of boundary layer velocity at +4° AOA and $Re_c = 46{,}000$

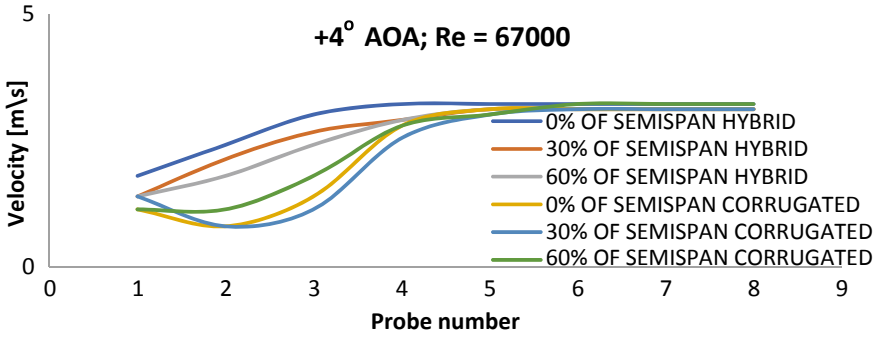

Fig. 14 Comparison of boundary layer velocity at +4° AOA and $Re_c = 67{,}000$

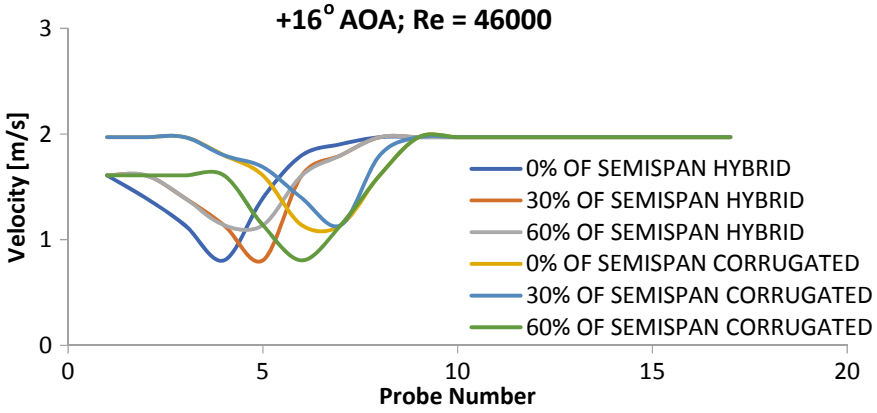

Fig. 15 Comparison of boundary layer velocity at +16° AOA and $Re_c = 46{,}000$

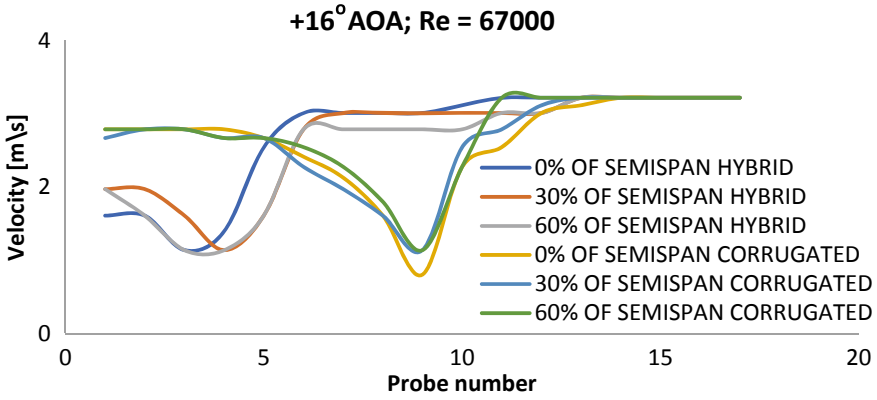

Fig. 16 Comparison of boundary layer velocity at +16° AOA and $Re_c = 67{,}000$

wing. This shows that at higher AoA the corrugated wing would perform better than the hybrid wings. The spanwise flow is also almost the same in the corrugated wing in this flow regime, which is not observed in hybrid wing (Fig. 15 and 16).

4 Conclusion

No flow reversal and flow separation are observed for the two wings at the Re_c 46,000 or 67,000 and AoA from $-8°$ to $+16°$. However, flow fluctuation in the hybrid wing found more than the corrugated wing.

At chord Reynold number 120,000, the flow reversal occurred in a hybrid wing at $+14°$ AoA and in corrugated wing it happened at $+18°$ AoA. This shows that the corrugated wing is 28% more efficient for delaying the stall of the wing.

The boundary layer measurement results also show the same trends, in which at higher AoA, the corrugated wing shows a lesser velocity gradient than the hybrid wing.

The corrugated wing is most suitable for higher AoA (28%) without facing flow separation and flow reversal.

The dragonfly bio-inspired corrugated wing is the most suitable for the future generation low speed micro air vehicle.

References

1. Estevez J, Lopez-Guede JM, Grana M (2015) Quasi-stationary state transportation of a hose with quadrotors. Robot Auton Syst 63:187–194. https://doi.org/10.1016/j.robot.2014.09.004; Mohiuddin T, Taha Y, Zweiri D, Gan (2019) UAV payload transportation via RTDP based optimized velocity profiles. Energies 12(16):30–49. https://doi.org/10.3390/en12163049
2. Wall Street Journal. Google drones can already deliver you coffee in Australia. Available online: https://www.youtube.com/watch?v=prhDrfUgpB0. Accessed on 6 Apr 2019
3. Mohiuddin A, Taha T, Zweiri Y, Gan D (2019) UAV payload transportation via RTDP based optimized velocity profiles. Energies 12(16):30–49. https://doi.org/10.3390/en12163049
4. Stolaroff JK, Samaras C, O'Neill ER, Lubers A, Mitchell AS, Ceperley D (2018) Energy use and life cycle greenhouse gas emissions of drones for commercial package delivery. Nat Commun 9:409
5. Liu J, Guan Z, Shang J, Xie X (2018) Analysis of environmental impacts of drone delivery on an online shopping system. J Syst Sci Inform 6(4):302–319. https://doi.org/10.21078/JSSI-2018-302-18
6. McMasters JH, Henderson ML (1980) Low speed single element airfoil synthesis. Tech Soaring 2(2):1–21
7. Carmichael BH (1981) Low Reynolds number airfoil survey, vol 1; NASA CR-165803; NASA, Washington, DC
8. Lissaman PBH (1983) Low-Reynolds-number airfoils. Annu Rev Fluid Mech 15:223–239
9. Gad-el-Hak M (2001) Micro-air-vehicles: can they be controlled better? J Aircr 38:419–429
10. Wakeling JM, Ellington CP (1997) Dragonfly flight. I. Gliding flight and steady-state aerodynamic forces. J Exp Biol 200:543–556

11. Kesel AB (2000) Aerodynamic characteristics of dragonfly wing sections compared with technical aerofoil. J Exp Biol 203:3125–3135. https://doi.org/10.1016/S0010-4825(98)018-3
12. Rees CJC (1975) Aerodynamic properties of an insect wing section and a smooth aerofoil compared. Nature 258:141–142
13. Brodsky AK (1994) The evolution of insect flight. Oxford University Press, Oxford, UK
14. Rudolph R (1978) Aerodynamic properties of Libellula quadrimaculata L. (Anisoptera: Libellulidae), and the flow around smooth and corrugated wing section models during gliding flight. Odonatologica 7:49–58
15. Okamoto M, Yasuda K, Azuma A (1996) Aerodynamic characteristics of the wings and body of a dragonfly. J Exp Biol 199:281–294
16. Luo G, Sun M (2005) The effects of corrugation and wing planform on the aerodynamic force production of sweeping model insect wings. Acta Mech Sin 21:531–541
17. Vargas A, Mittal R (2004)Aerodynamic performance of biological airfoils. In: Proceedings of 2nd flow control conference, Portland, Oregon AIAA2004-2319. https://doi.org/10.2514/6.2004-2319
18. Murphy J, Hu H (2010) An experimental study of a bio inspired corrugated airfoil for micro air vehicle applications. Exp Fluids 492:531–546. https://doi.org/10.1007/s00348-010-0826-z
19. Tang H, Lei Y, Li X, Fu Y (2019) Numerical investigation of the aerodynamic characteristics and attitude stability of a bio-inspired corrugated airfoil for MAV or UAV applications. Energies 12:4021. https://doi.org/10.3390/en12204021
20. Dwivedi YD, Bhargava V, Rao PMV, Jagadeesh D (2019) Aerodynamic performance of micro aerial wing structures at low Reynolds number. INCAS Bulletin 11(1):107–120. https://doi.org/10.13111/2066-8201.2019.11.1.8
21. Dwivedi YD, Sudhir Sastry YB (2019) An experimental Flow field study of a bio-inspired corrugated wing at low Reynolds number. INCAS Bulletin 11(3):55–65. https://doi.org/10.13111/2066-8201.2019.11.3.5
22. Dwivedi YD, Ho WH, Rao PMV (2017) Spanwise flow analysis of gliding bio-inspired corrugated wing. J Adv Res Dyn Control Syst 12-Special issue
23. Dwivedi YD (2017) Effect of peak shape in bio inspired corrugated wing. In: International conference on advances in thermal systems, materials and design engineering (ATSMDE2017), VJTI, Mumbai
24. Tamai M, Wang Z, Rajagopalan G, Hu H, He G (2007) Aerodynamic performance of a corrugated dragonfly airfoil compared with smooth airfoils at low Reynolds numbers. In: 45th AIAA aerospace sciences meeting and exhibit, pp 1–12
25. Skote M (2014) Scaling of the velocity profile in strongly drag reduced turbulent flows over an oscillating wall. I J Heat Fluid Flow 50:352–358
26. Skote M (2011) Turbulent boundary layer flow subjected to stream wise oscillation of spanwise wall-velocity. Phys Fluids 23:1701–1704
27. Chen YH, Skote M (2016) Gliding performance of 3-D corrugated dragonfly wing with spanwise variation. J Fluids Struct 62:1–13